Results in Chemistry 4 (2022) 100375

Contents lists available at ScienceDirect

Results in Chemistry

journal homepage: www.sciencedirect.com/journal/results-in-chemistry

PtSb/C electrocatalysts for glycerol oxidation in alkaline electrolyte

C.V. Pereira [a], V.A. Maia [a], P.J. Zambiazi [a], R.F.B. de Souza [a], E. Antolini [b], A.O. Neto [a,*]

[a] Instituto de Pesquisas Energéticas e Nucleares, IPEN-CNEN/SP, Cidade Universitária, 05508-900 São Paulo, SP, Av. Prof. Lineu Prestes, 2242, Brazil
[b] Scuola di Scienza dei Materiali, Via 25 aprile 22, Cogoleto, 16016 Genova, Italy

ARTICLE INFO

Keywords:
Glycerol oxidation reaction
PtSb
Fuel cell
Chemicals and products

ABSTRACT

Pt/C and PtSb/C catalysts in various atomic ratios were synthesized by the sodium borohydride reducing method and their activity for the glycerol oxidation reaction (GOR) was evaluated in alkaline media. Transmission Electron Microscopy (TEM) images showed that Pt particle size increases with increasing Sb content in the catalyst. X-ray photoelectron spectroscopy (XPS) showed that the ratio of Pt and Sb is close to that expected. By XPS measurements, the presence of Sb_2O_5 in $Pt_{70}Sb_{30}$/C and $Pt_{50}Sb_{50}$/C was observed. X-ray diffraction (XRD) analysis revealed the presence of the face-centered cubic (FCC) structure of Pt and PtSb and of some others phases that could be identified as Sb oxides. By linear sweep voltammetry (LSV) measurements, $Pt_{80}Sb_{20}$/C showed the highest activity for the GOR in alkaline media for potentials >-0.35 V *vs.* Ag/AgCl, while $Pt_{50}Sb_{50}$/C showed the highest GOR activity in the potential range between -0.60 and -0.35 V *vs.* Ag/AgCl. The direct glycerol fuel cells with $Pt_{80}Sb_{20}$/C as the anode catalyst showed the best performance. These results attest the beneficial effect of Sb addition to platinum: the activity enhancement in the presence of Sb atoms has to be ascribed to both a bifunctional mechanism related to the presence of Sb oxides, and an electronic effect between platinum and antimony in the PtSb alloy.

1. Introduction

Direct glycerol fuel cells (DGFC) attract great interest from the scientific community for making use of a non-toxic, non-volatile, non-flammable, bio renewable fuel alcohol, in addition to having a high boiling point (290 °C), relatively high energy density (6260 kWh L^{-1}) when compared to other fuels such as ethanol (5442 kWh L^{-1}) and methanol (4047 kWh L^{-1}) [1,2].

Being available as an inevitable by-product in the biodiesel manufacturing process, glycerol becomes an excess and low-cost raw material, making its study an advantage both for energy purposes [3] and for the value-added synthesis molecules [4–5], such as dihydroxyacetone, glyceraldehyde, glycerate, hydroxypyruvate, tartronate, glycolate and oxalate [4,6]. In particular, dihydroxyacetone is a potentially important chemical in the cosmetic industry used in the production of degradable polymers [3–4,7].

The oxidation of alcohol in alkaline media presents some advantages than in acid media, as an easily deprotonation and a decrease in the number of intermediates due to instability of aldehydes, resulting in a more complete oxidation of the fuel [8]. Pt and Pd are commonly used as catalysts for alcohol oxidation in alkaline media. In this context, Pt and Pd can benefit from the addition of a second metal, which can promote/depress the breaking of the C–C bond [9].

The addition of Sb to Pt enhances the water activation at low potentials, kinetically favoring the oxidation of alcohols, as the oxygenated species generated in this process react very strongly with the species adsorbed on platinum, transferring electrons very quickly. Zhang and Xia [10] reported that PtSb/C catalysts are more active for methanol oxidation than Pt/C. Xingwen and Peter [11] showed that PtSb/C catalysts are a higher activity than Pt/C for formic acid oxidation. Two works were addressed to the use of a supported PtSb catalyst for the glycerol oxidation [3,12]. Nie et al. [12] reported the selective oxidation of glycerol to dihydroxyacetone (DIHA) in a base-free aqueous solution using multiwall carbon nanotubes (MWCNTs) supported PtSb alloy nanoparticles.

An advantage of PtSb/MWCNTs catalyst is that the serious C–C cleavage reaction over monometallic Pt/MWCNTs and Pt-Bi/MWCNTs is depressed. Lee et al. [3] reported the partial electrooxidation of glycerol on PtSb/C in an acidic solution to produce value-added chemicals, such as dihydroxyacetone (DHA), glyceraldehyde (GAD), glyceric acid (GLA), and glycolic acid (GCA). In both these works only one PtSb composition was investigated. In this work PtSb/C were prepared in

* Corresponding author.
E-mail address: aolivei@usp.br (A.O. Neto).

https://doi.org/10.1016/j.rechem.2022.100375
Received 19 April 2022; Accepted 17 May 2022
Available online 20 May 2022
2211-7156/© 2022 The Author(s). Published by Elsevier B.V. This is an open access article under the CC BY-NC-ND license (http://creativecommons.org/licenses/by-nc-nd/4.0/).

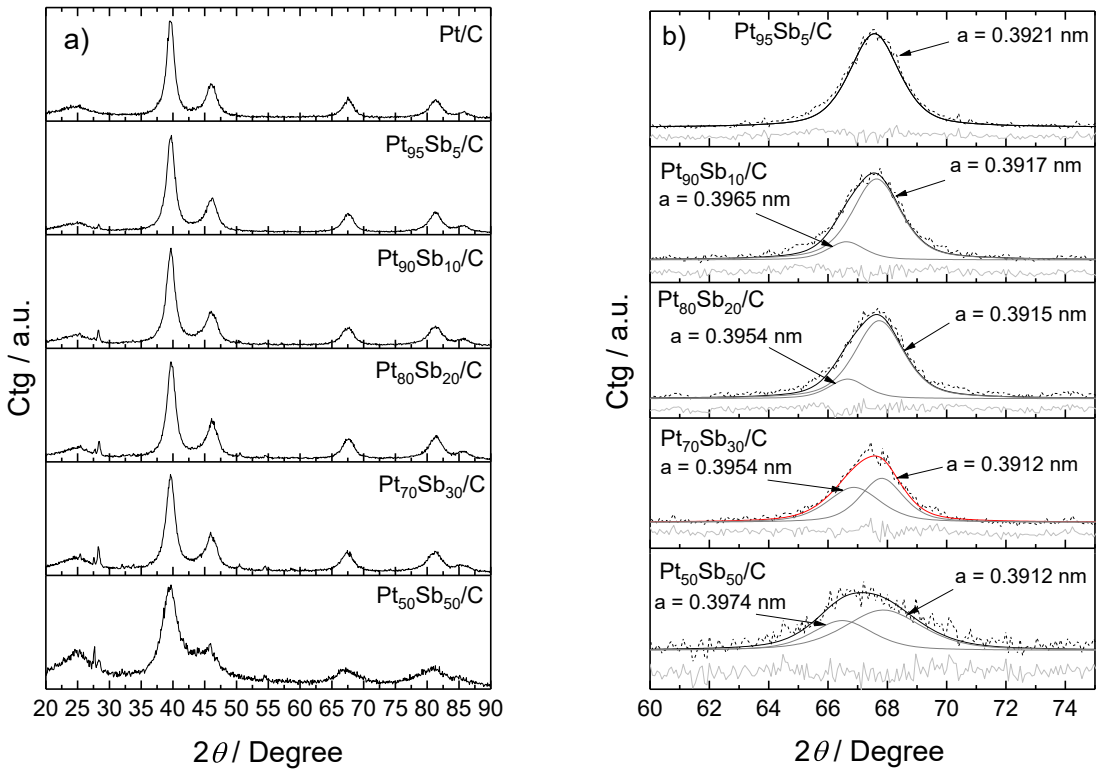

Fig. 1. a) XRD measurements for Pt/C and PtSb/C for 2θ from up to 20° to 90°. b) phases deconvolved by Pauly refinement with dash line for measures, black line for fitted, grey for phases and light grey for residual line.

different atomic ratios, and their activity for glycerol electrooxidation was evaluated in alkaline media.

2. Experimental

PtSb/C catalysts were prepared by borohydride reduction process [13] with 20% by mass and with 80% of Vulcan carbon XC 72 as support. The Vulcan XC 72 carbon support and the metallic precursors, $H_2PtCl_6{\cdot}6H_2O$ (Aldrich) and antimony acetate (Aldrich), were added in an isopropyl alcohol/water solution with a volumetric ratio equal to 50/50 (v/v). An aqueous solution of borohydride was added in a single step and the mixture was stirred for 30 min at room temperature. After the end of stirring, the suspension was filtered and the resulting product washed with water to remove impurities the soluble precursors, and finally dry in the oven at 70 °C.

The electrocatalysts were characterized by X-ray diffraction using a Rigaku Miniflex II diffractometer with Cu Kα source (λ = 1.54056 Å) at 2θ = 20° to 90° with a step size of 0.02° and a scan time of 2 s per step. Transmission electronic Microscopy was performed using JEOL electron microscope model JEM-2100. X-ray excited photoelectron spectroscopy (XPS) measurements were performed by a Thermo Scientific K-Alpha + monochromatic spectrometer with an Al Kα X-ray radiation source (hν = 1486.6 eV) where the depth of penetration was about 5 nm and spot size were set to 400 μm, which turns out to give information about the surface composition of the electrocatalysts peak energies were given to an accuracy of 0.1 eV and peak areas were normalized using appropriate atomic sensitivity factors. The spectra were deconvoluted and optimized using a Levenberg-Marquardt algorithm with U2 Tougaard and Shirley-type background in Casa XPS software.

The electrochemical studies in cyclic voltammetry and chronoamperometry were carried out in the Autolab PGSTAT 30 potenciostat/galvanostat in solutions with concentrations of 1.0 mol L^{-1} of glycerol in the presence of a 1 mol L^{-1} solution of NaOH. The results were obtained in conventional electrochemical cells. A thin porous coating was used as a working electrode, platinum plate as a counter electrode and an Ag/AgCl electrode (3.0 mol L^{-1} KCl) as a reference electrode. Cyclic voltammograms are obtained at a potential of –0.85 V to 0.2 V at a speed of 10 mV s^{-1}. For studies with the chronoamperometry technique, the potential was set at −0.4 V for 1800 s. During all experiments the solution was constantly saturated with N_2 (gaseous).

The spectro-electrochemical ATR-FTIR *in situ* measurements were performed with a Nicolet 6700 FT-IR spectrometer with a MCT detector cooled with liquid N_2, ATR accessory (MIRacle with a Diamond/ZnSe Crystal Plate Pike®) and an electrochemical cell better explained in the literature [14–16]. The same working electrodes of electrochemical experiments were used in presence of 1.0 mol L^{-1} glycerol + 1 mol L^{-1} NaOH. The Raman spectro-electrochemical experiments were carryout using a three electrodes electrochemical cell adapted inside MacroRam Raman spectroscopy equipment (Horiba Scientific) in the same conditions of ATR-FTIR experiments.

For Direct alkaline glycerol fuel cells was utilized a Nafion® 117 membrane (DuPontTM) as electrolyte, the diffusion layer (GDL) uses the backbone of carbon cloth (EC-CC1-060T) treated with 10% PTFE supplied by ElectroChem Inc. The catalytic layer of the cathode was prepared using commercial catalyst Pt/C E-TEK (20% Pt by mass, batch: C0740621) with 1 mg of Pt cm^{-2} and 30% of Nafion, while for the preparation of the catalytic layer of the anode, 1 mgPt cm^{-2} of the

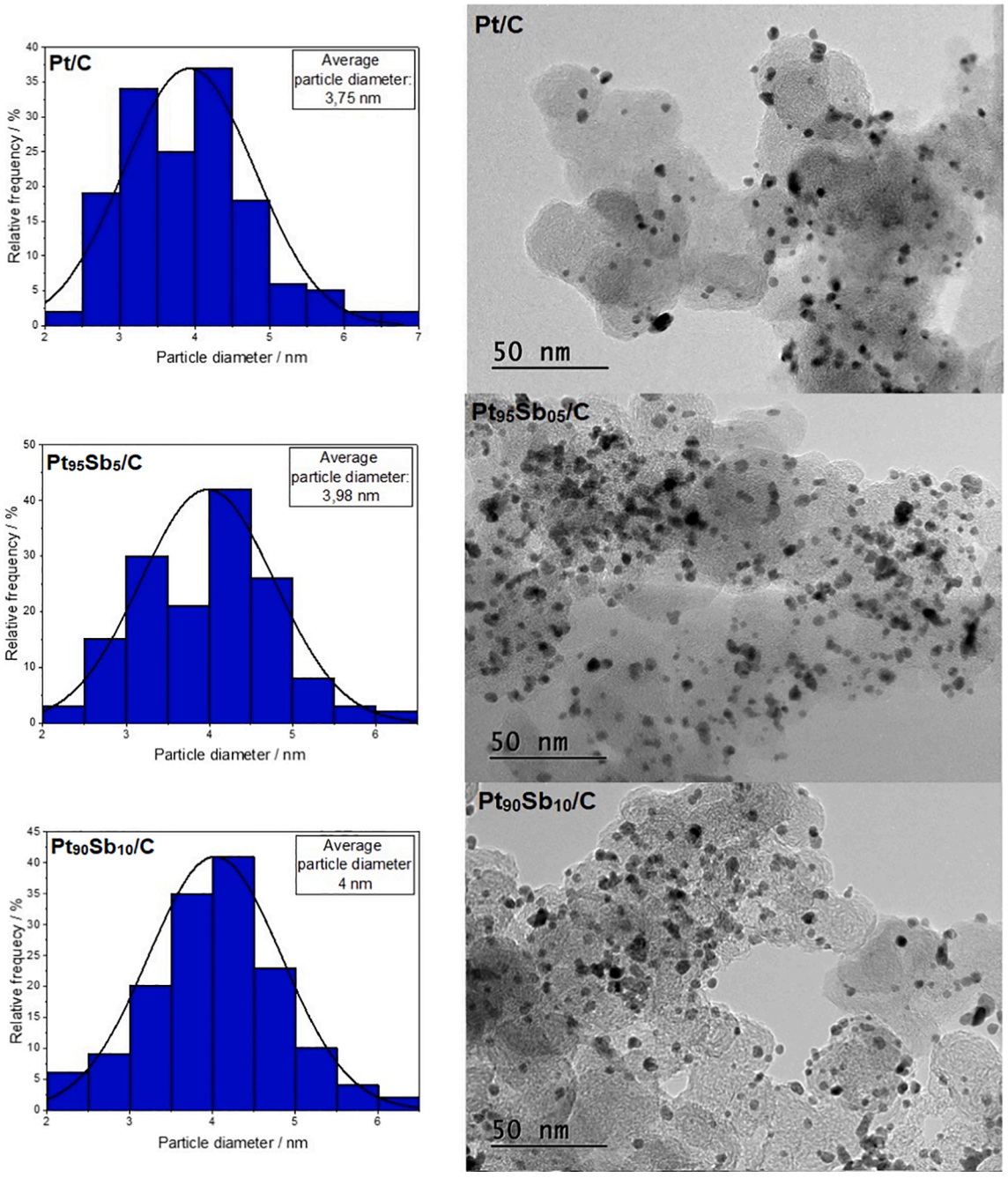

Fig. 2. (a) Micrographs obtained by transmission electron microscopy analysis and histograms $Pt_{50}Sb_{50}/C$. (b) Dependence of Pt particle size on Sb content in the catalyst.

electrocatalysts prepared and 30% Nafion® (5% DE520 dispersion from DuPontTM). The catalytic layers were applied manually on the carbon fabric by the brush painting technique until the total transfer of the catalytic charge. Before making the MEA, the polymeric membrane Nafion® was previously subjected to a 6 mol L^{-1} NaOH solution for 24 h. After this procedure, the electrodes were pressed together with the Nafion® membrane, at 125 °C for 10 min at a pressure of 225 kgf cm^{-2}. The tests for the polarization measurements were performed by a Cell unit with serpentine graphite plates with a geometric area of 5 cm^2. The anode was fed by a flow of 1 mL min^{-1} of a 2.0 mol L^{-1} NaOH solution in the presence of 2.0 mol L^{-1} glycerol. The cathode was kept under an oxygen flow of 150 mL min^{-1}. The polarization curves were presented from the average results of three tests performed [17].

3. Results and discussion

XRD measurements Pt/C, $Pt_{50}Sb_{50}/C$, $Pt_{70}Sb_{30}/C$, $Pt_{80}Sb_{20}/C$, $Pt_{90}Sb_{10}/C$ and $Pt_{95}Sb_5/C$ for 2θ from 20° to 90° are showed in Fig. 1a. All electrocatalysts showed a diffraction peak near 2θ = 25° referring to the Vulcan XC 72 carbon support, others peaks that appeared at approximately 2θ = 40°, 46°, 67°, 80° and 87° are associated with the planes (1 1 1), (2 0 0), (2 2 0), (3 1 1) and (2 2 2) characteristic of platinum associated to face-centered cubic structure. The diffraction peaks at ≈ 27°, 31°, 45° and 55° relative to the Sb_2O_3 phase (JCPDS # 5–534). A broadening of the Pt peak at 67° with increasing Sb content in the catalyst and a shift of the peak to lower 2*θ*, indicating the expansion of lattice parameter, were observed, maybe due to the segregation of a Pt

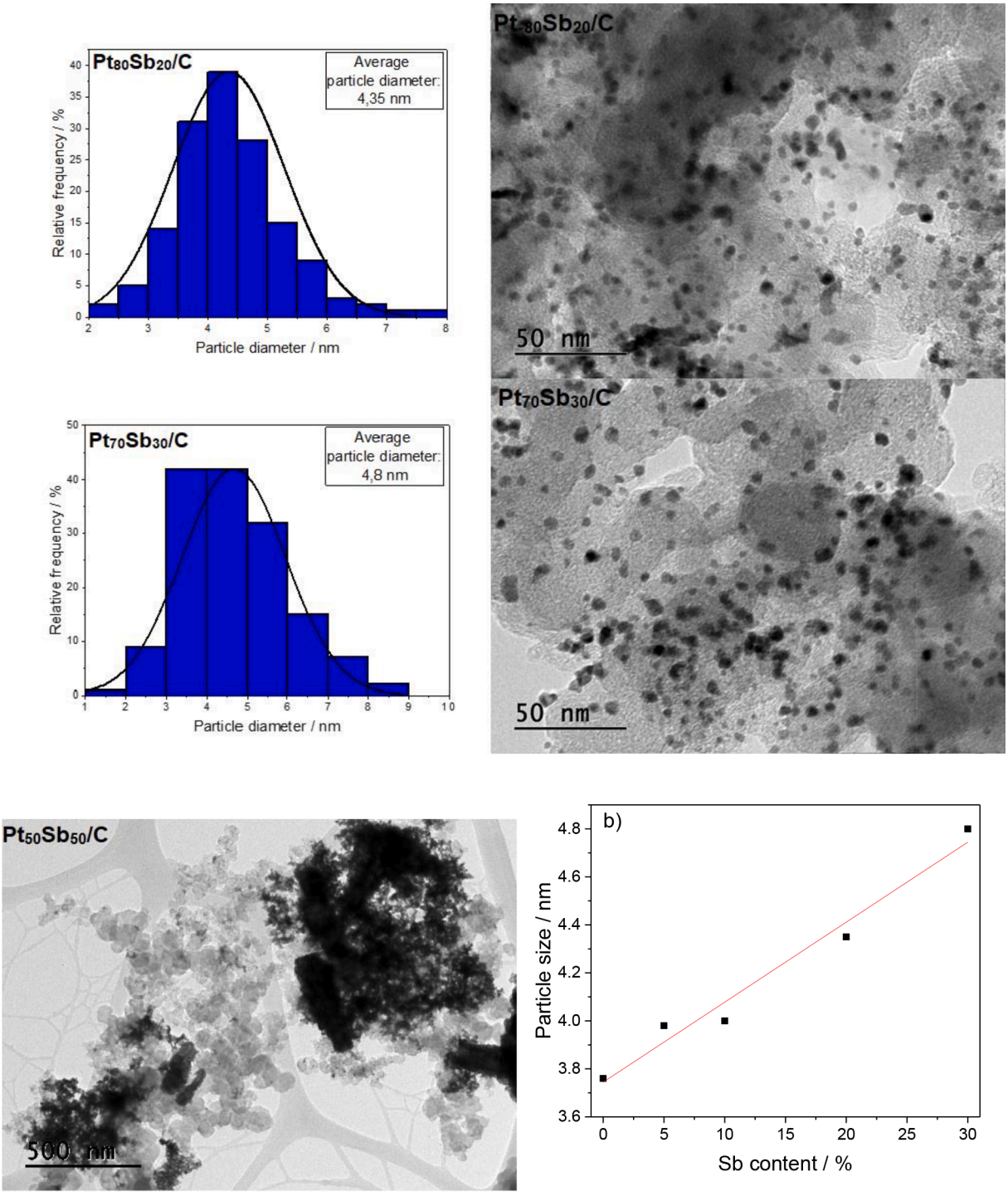

Fig. 2. (*continued*).

phase (at ~ 0.391 nm) and the formation of a PtSb phase alloy with Sb incorporated in Pt lattice (Fig. 1b).

The micrographs obtained by transmission electron microscopy analysis and histograms for Pt/C, $Pt_{50}Sb_{50}$/C, $Pt_{70}Sb_{30}$/C, $Pt_{80}Sb_{20}$/C, $Pt_{90}Sb_{10}$/C and $Pt_{95}Sb_{5}$/C are shown in Fig. 2a. It was noted that Pt-Sb materials showed good dispersion, except the $Pt_{50}Sb_{50}$/C electrocatalyst, which showed a large number of agglomerations on the carbon support. This result is accordance with reported by Ayoub et al. [18], the high agglomeration, which may also be due to the ripening effect [19], where smaller particles with greater surface energy dissolved with subsequent re-precipitation and formation of larger particles. The dependence of Pt particle size on Sb content in the catalyst is shown in Fig. 2b. An almost linear increase of the average Pt particle size with increasing Sb content in the catalyst can be observed in Fig. 2b.

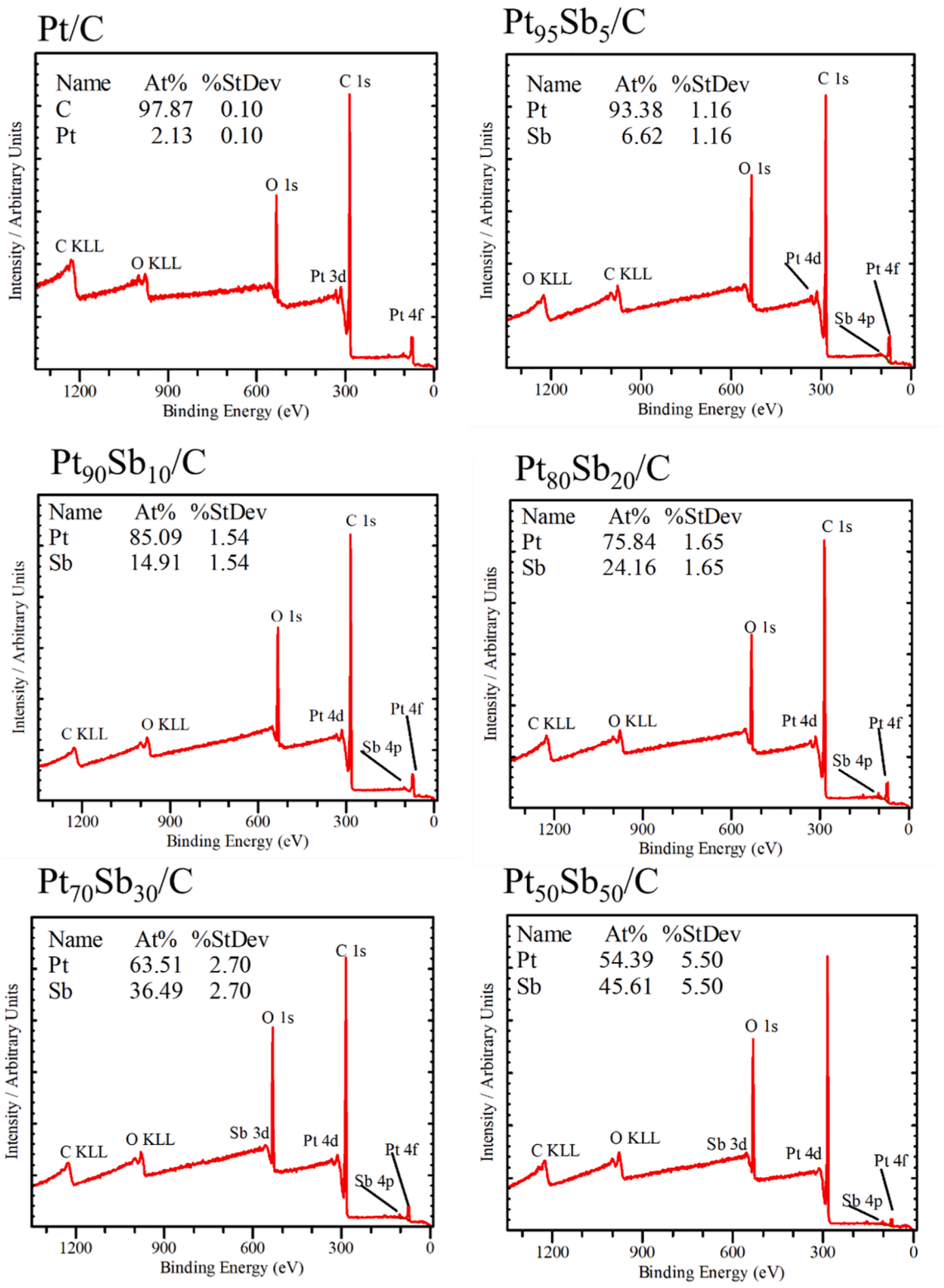

Fig. 3. XPS survey scans of electrocatalyst in full spectrum with the ratio of surface metals.

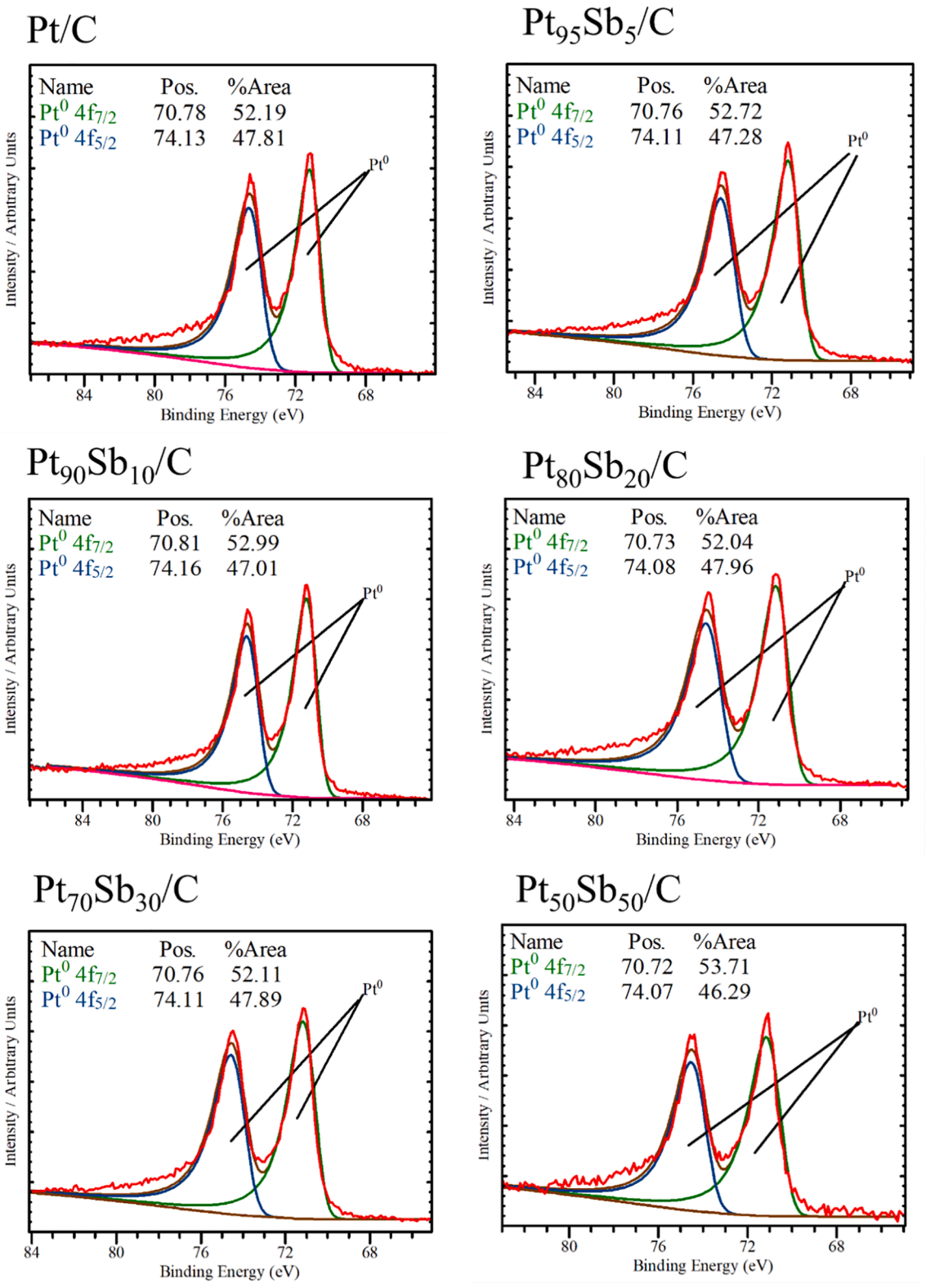

Fig. 4. High resolution spectra detailing the Pt $4f_{7/2}$ and Pt $4f_{5/2}$ to electrocatalyst.

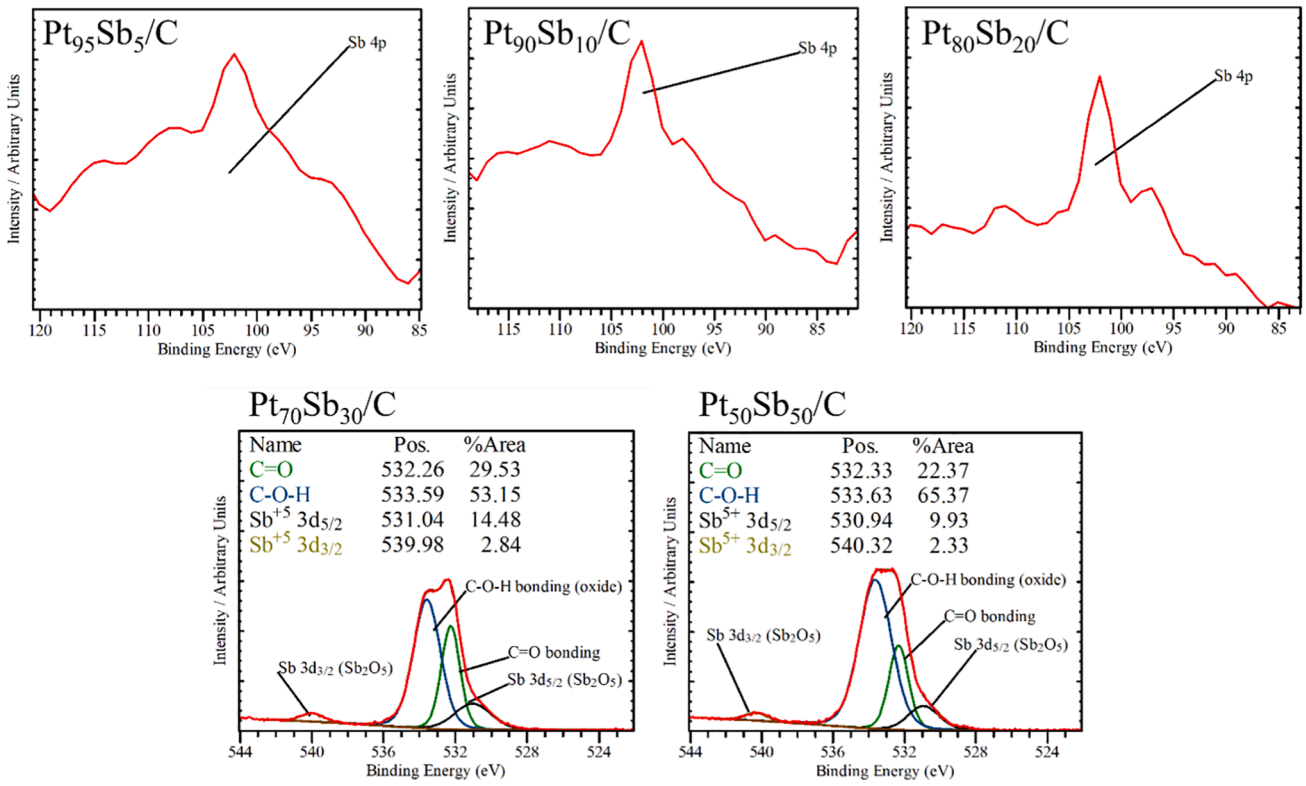

Fig. 5. High resolution spectra detailing the Sb $3d_{5/2}$ and Sb $3d_{3/2}$ to electrocatalyst.

Table 1
Elemental analysis of the metals by XPS indicated that the ratio of Pt and Sb.

Electrocatalyst	Pt (% mass)	Sb (% mass)
Pt/C	24.9 ± 0.1*	n.d.**
$Pt_{95}Sb_5$/C	95.5 ± 1.2	4.5 ± 1.2
$Pt_{90}Sb_{10}$/C	90.1 ± 1.5	9.9 ± 1.5
$Pt_{80}Sb_{10}$/C	83.5 ± 1.6	16.5 ± 1.6
$Pt_{70}Sb_{30}$/C	73.7 ± 2.7	26.3 ± 2.7
$Pt_{50}Sb_{50}$/C	65.8 ± 5.5	34.2 ± 5.5

*Compared with Carbon; **n.d. = Not determined.

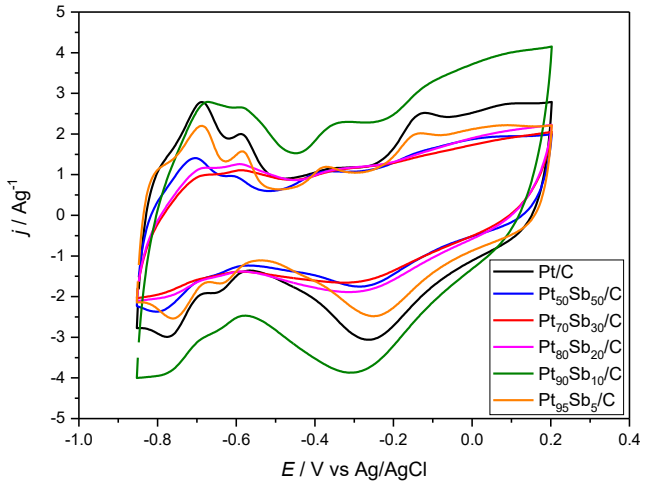

Fig. 6. Cyclic voltammetry in 1 mol/L of NaOH for Pt/C, $Pt_{50}Sb_{50}$/C, $Pt_{70}Sb_{30}$/C, $Pt_{80}Sb_{20}$/C, $Pt_{90}Sb_{10}$/C and $Pt_{95}Sb_5$/C electrocatalysts V = 10 mV/s.

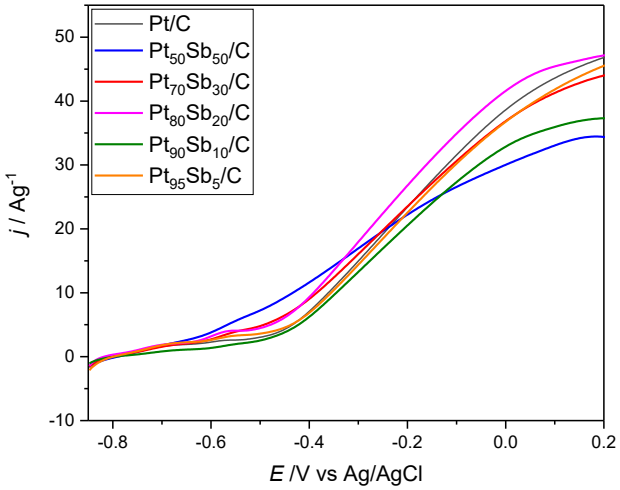

Fig. 7. LSV measurement in presence of 1 mol L^{-1} of NaOH + 1 mol L^{-1} of glycerol for Pt/C, $Pt_{50}Sb_{50}$/C, $Pt_{70}Sb_{30}$/C, $Pt_{80}Sb_{20}$/C, $Pt_{90}Sb_{10}$/C and $Pt_{95}Sb_5$/C electrocatalysts V = 10 mV/s.

XPS patterns of the Pt/C and PtSb/C catalysts are shown in Figs. 3–5. Fig. 3 shows complete spectra of the Pt/C and PtSb/C indicating the presence of the elements and the percentage of atoms present in the electrocatalysts. Elemental analysis of the metals by XPS indicated that the ratio of Pt and Sb is close to that expected, except $Pt_{50}Sb_{50}$/C, as shown in Table 1. The lower amount of Sb in the $Pt_{50}Sb_{50}$/C catalyst could be due to Pt segregation on the catalyst surface.

High-resolution spectrum analysis of Pt 4f exhibited a characteristic spin–orbit doublet of Pt^0 (71.0 eV) and Pt^0 (74.3 eV) [20] in all synthesized electrocatalysts, as shown in Fig. 2. The peaks Pt 4f shows an

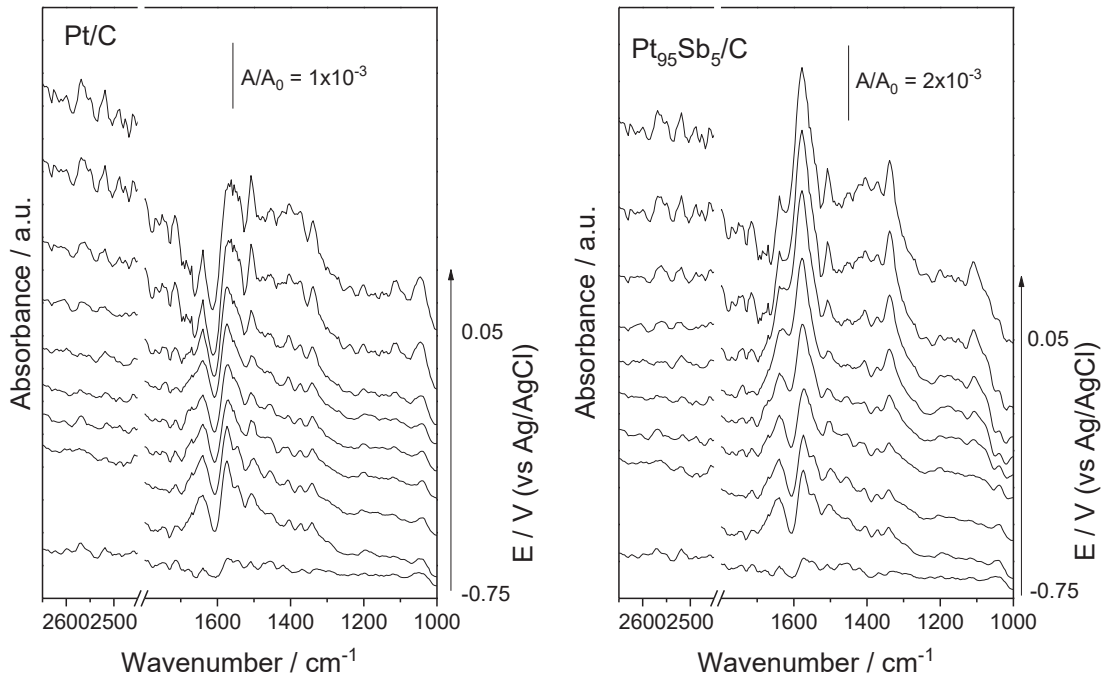

Fig. 8. *In-Situ* ATR-FTIR spectra of electrochemical measurements of glycerol oxidation reaction in NaOH 1.0 mol L^{-1} + glycerol 1.0 mol L^{-1} on PtSb/C materials taken at −0.75 to 0.05 V. Backgrounds collected at −0.85 V.

asymmetric peak-shape and were fitted using the is splitting distance of 3.35 eV.

The high resolution spectra of Sb $3d_{5/2}$, around 528.0–531.5 eV, are overlapped on those of O 1 s (531–534 eV) [21]. Due to low Sb concentration in the $Pt_{95}Sb_5$/C, $Pt_{90}Sb_{10}$/C, $Pt_{80}Sb_{20}$/C electrocatalyst, it was not possible to identify the presence of Sb oxide nor metallic in Sb 3d binding energy region. Therefore, for these three electrocatalysts we use the Sb 4p peaks present in the spectrum about 102.0 eV to confirm this element, as show Fig. 4 [22].

However, for the electrocatalysts $Pd_{70}Sb_{30}$/C and $Pd_{50}Sb_{50}$/C it was possible to detect the presence of Sb 3d as shown in Fig. 3b. The high-resolution spectra to these electrocatalysts show a spin–orbit doublet Sb^{+5} $3d_{5/2}$ and Sb^{+5} $3d_{3/2}$ with an energy separation of 9.35 eV [23]. We use to fit and constrain the Sb $3d_{3/2}$ peaks as a guide. The component in the spectrum at 533 eV is associated with carbon–oxygen binding in organic species which is present in the carbon black support [24]. While the component in 532 eV is related to O bound to metal oxides, in corroboration to the presence of Sb_2O_5 [25,26]. The spectra of Fig. 5 reinforce the presence of Sb_2O_5.

Cyclic voltammograms of Pt/C, $Pt_{50}Sb_{50}$/C, $Pt_{70}Sb_{30}$/C, $Pt_{80}Sb_{20}$/C, $Pt_{90}Sb_{10}$/C and $Pt_{95}Sb_5$/C in presence of 1 mol L^{-1} of NaOH are shown in Fig. 6. $Pt_{50}Sb_{50}$/C, $Pt_{70}Sb_{30}$/C, $Pt_{80}Sb_{20}$/C showed an adsorption region (between −0.85 and −0.5 E/V *vs* Ag/AgCl) with lower current values in comparation to the Pt/C electrocatalyst. This is probably due to the overlay of platinum sites by Sb, hindering hydrogen adsorption. This region is less defined as Sb loads increase, indicating a possible higher formation of antimony oxides over Pt sites [27]. The $Pt_{95}Sb_5$/C electrocatalyst showed better defined hydrogen adsorption/desorption regions when compared to the Pt/C electrocatalyst. The $Pt_{90}Sb_{10}$/C electrocatalyst showed an increase in current in relation to the Pt/C electrocatalyst however the hydrogen adsorption/desorption regions are slightly less defined.

Linear sweep voltammetry (LSV) in 1 mol L^{-1} of NaOH + 1 mol L^{-1} of glycerol for Pt/C, $Pt_{50}Sb_{50}$/C, $Pt_{70}Sb_{30}$/C, $Pt_{80}Sb_{20}$/C, $Pt_{90}Sb_{10}$/C and $Pt_{95}Sb_5$/C electrocatalysts are shown in Fig. 7. The electro-oxidation of glycerol on the Pt/C, $Pt_{70}Sb_{30}$/C, $Pt_{80}Sb_{20}$/C, $Pt_{90}Sb_{10}$/C and $Pt_{95}Sb_5$/C electrocatalysts started at approximately −0.57 V *vs.* Ag/AgCl, while on $Pt_{50}Sb_{50}$/C electrocatalyst it started at a potential of approximately −0.65 V *vs.* Ag/AgCl. In the range −0.60–0.35 V *vs.* Ag/AgCl $Pt_{50}Sb_{50}$/C showed the highest current, while for potential >−0.35 V *vs.* Ag/AgCl the highest current was shown by the $Pt_{80}Sb_{20}$/C catalyst.

To understands the process of glycerol oxidation reaction on the PtSb catalyst, was taken spectra of in-situ ATR-FTIR spectroscopy (Fig. 8). For all materials it was observed the consumption of glycerol at 1004, 1041 and 1094 cm^{-1} bands [28,29], moreover for $Pt_{50}Sb_{50}$/C, $Pt_{80}Sb_{20}$/C, and $Pt_{90}Sb_{10}$/C these bands were negatively shifted. It was also observed bands related to glyceraldehyde at 1077 cm^{-1} [30], formate at 1228 cm^{-1} [31], 1,3-dihydroxy-2-propanone at 1333 cm^{-1} [32], tartronate at 1348 cm^{-1} [33], hydroxypyruvate at 1359 cm^{-1} [28,29], glycerate at 1375 cm^{-1} [32,34,35], carbonate at ~1405 cm^{-1} [28], carbonyl and carboxyl stretches at ~1665 cm^{-1} [28,34], oxalate at 1620 cm^{-1} [6] and glycerate at 2550 cm^{-1} [36,37].

The literature [6,32,35,38–40] points out that the oxidation of this alcohol in an alkaline medium has many possibilities of parallel pathways, as shown in Fig. 9, and, by the appearance of the species noticed by the FTIR spectra, it is possible to trace the preferred path of each catalyst.

To better observe the reaction pathways, the band appointed was deconvolved in Lorentzian functions (Fig. 10), the first reaction step maintaining 3 carbons starts preferentially with 1,3-dihydroxy-2-propanone, appearing so close to the onset potential observed in voltammetry (Fig. 7), with an ever-increasing profile for all materials. However, the glyceraldehyde also pointed out as a possible first step appears close to the onset potential for materials containing higher proportions of Pt,

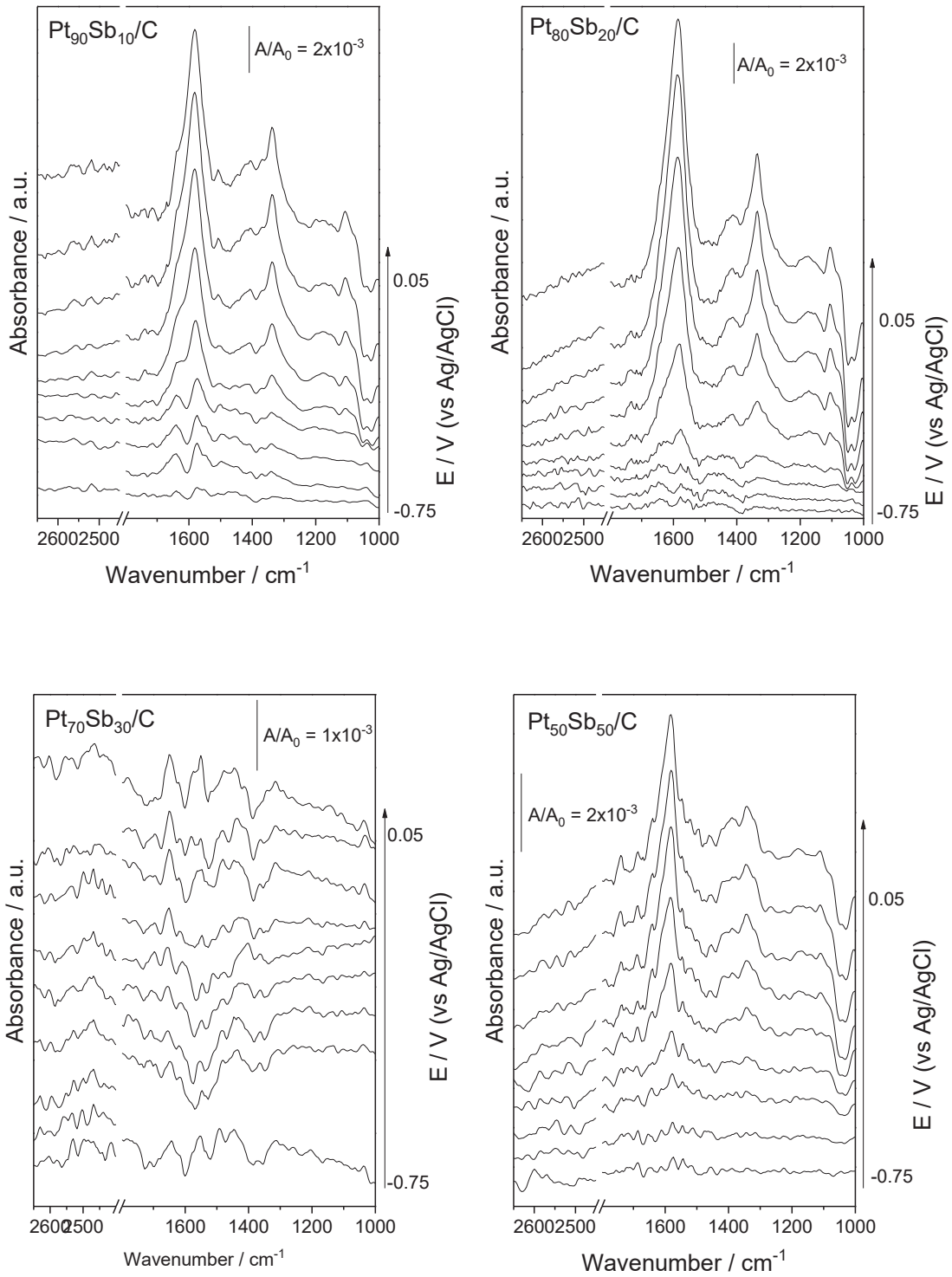

Fig. 8. (*continued*).

such as Pt/C, $Pt_{95}Sb_5$/C and $Pt_{90}Sb_{10}$/C. For $Pt_{80}Sb_{20}$/C and $Pt_{50}Sb_{50}$/C this band is not observed.

Notably, for $Pt_{70}Sb_{30}$/C this band appears late, close to −0.35 V probably due to the accumulation of species shifting the equilibrium with 1,3-dihydroxy-2-propanone, in agreement with Fontes et al [6], reporting that 1,3-dihydroxy-2-propanone is more stable in alkaline media, for more instable compound. This tendency towards the glyceraldehyde pathway is only confirmed by the data from the integration of the glycerate and glycolate bands, which would be the next step of the reaction.

Hydroxypyruvate is observed for all catalysts except for the $Pt_{70}Sb_{30}$/C composition, indicating that this material may be supports the breakage of the 3-carbon chain before the others. For this material, the production of oxalate and carbonate is notable in more negative potentials than for the other materials.

To better understand the relationship between the catalytic surface and the products formed, in-situ RAMAN spectroscopy-assisted electrochemical experiments were performed in the presence of glycerol (Fig. 11) and large bands at 794, 974, and 1.166 cm^{-1} corresponding to ν(C–S), ν_s(C–O–C) and ν (CF_2) of Nafion® [41] were observed.

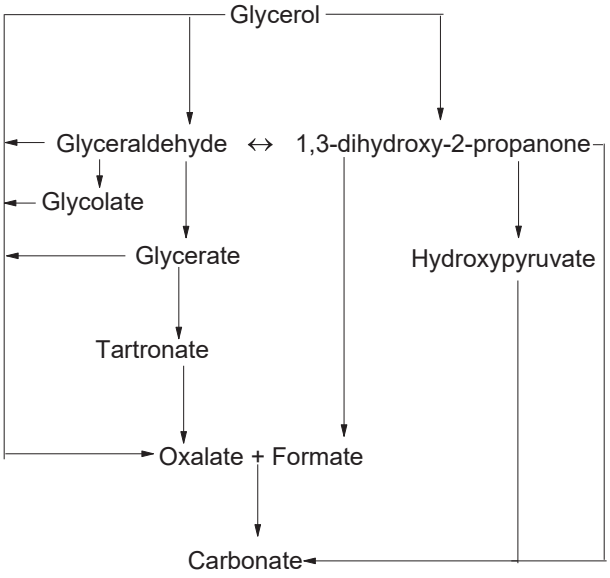

Fig. 9. Glycerol oxidation reaction pathways in alkaline media.

In all Raman spectra, the band referring to PtO_x ~ 599 cm^{-1} [42] and its evolution with increasing potential is also observed. In the Pt/C spectra, the band at 706 cm^{-1} is also observed, corresponding to that observed by Graham [43] for the Pt_3O_4 phase, however the presence of Sb seems to inhibit platinum to be oxidized to this phase, as it is not seen in any of the Sb-containing materials, even in small proportions. In materials containing Sb the bands corresponding to Pt_5O_6 located at ~635 and 670 cm^{-1} [43] are observed, indicating that platinum is less oxidized in the presence of antimony, which is more oxophilic. This fact confirmed that in materials containing Sb, the band at ~831 cm^{-1} corresponding to Sb_2O_3 [44] increases its intensity with the potential, indicating an enrichment of oxygen with increasing potential: this could be explain the inhibition of the Pt_3O_4 phase.

Fig. 12a shows the current density/voltage and current density/power density plots for the direct glycerol fuel cells with Pt/C, $Pt_{50}Sb_{50}$/C, $Pt_{70}Sb_{30}$/C, $Pt_{80}Sb_{20}$/C, $Pt_{90}Sb_{10}$/C and $Pt_{95}Sb_5$/C anode electrocatalysts. The $Pt_{95}Sb_5$/C and $Pt_{80}Sb_{20}$/C electrocatalysts showed the highest open circuit potential with values of 1048 mV and 1024 mV, respectively. The Pt/C electrocatalyst presented an open circuit potential of 945 mV, higher than the other compositions $Pt_{90}Sb_{10}$/C, $Pt_{70}Sb_{30}$/C and $Pt_{50}Sb_{50}$/C. The dependence of the maximum power density on Sb content in PtSb/C catalyst is shown in Fig. 12b. A maximum of the curve can be observed at 25 wt% Sb. The activity enhancement in the presence of Sb atoms has to be ascribed to both a bifunctional mechanism related to the presence of Sb oxides, and an electronic effect between platinum and antimony in the PtSb alloy. The bifunctional mechanism is based on the enhancement of poison species oxidation rate by Sb oxides. Electronic effects of Sb on Pt can affect H_2O dissociation, Pt–poison species bond strength and glycerol adsorption/dehydrogenation. The decrease of the performance for Sb contents >25 wt% has to be ascribed to the higher Pt particle size, decreasing Pt active sites, the greater thickness of the catalytic layer and the presence of a higher amount of Sb oxides, hindering reactants flow.

4. Conclusion

Pt/C and PtSb/C with various atomic ratios were successfully synthesized by the sodium borohydride reduction method. The XRD and XPS measurements indicated the presence of Sb oxides. $Pt_{80}Sb_{20}$/C showed the best results in LSV measurements for potentials > −0.35 V *vs.* Ag/AgCl and in direct glycerol fuel cells in alkaline electrolyte. The higher activity of $Pt_{80}Sb_{20}$/C and $Pt_{70}Sb_{30}$/C than that of Pt/C effect has to be ascribed to the bifunctional mechanism related to the presence of

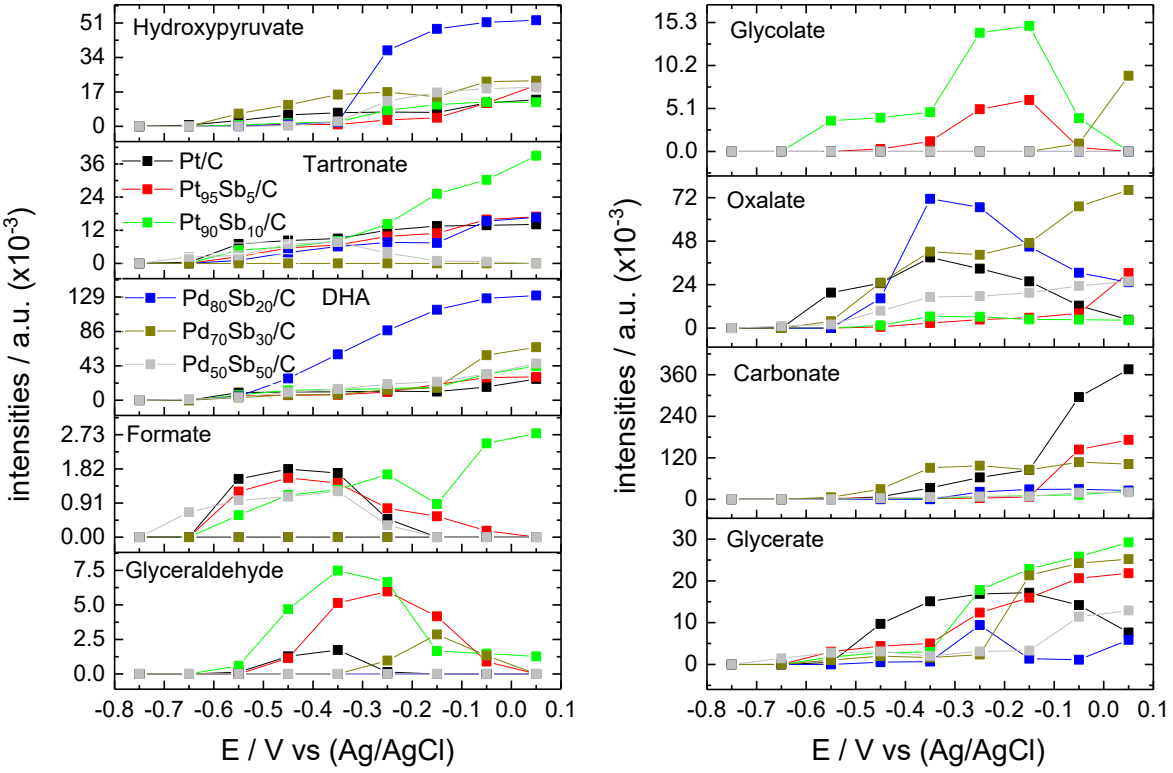

Fig. 10. Integrated Intensities bands as a function of the applied bias voltage. Data extracted from Fig. 8.

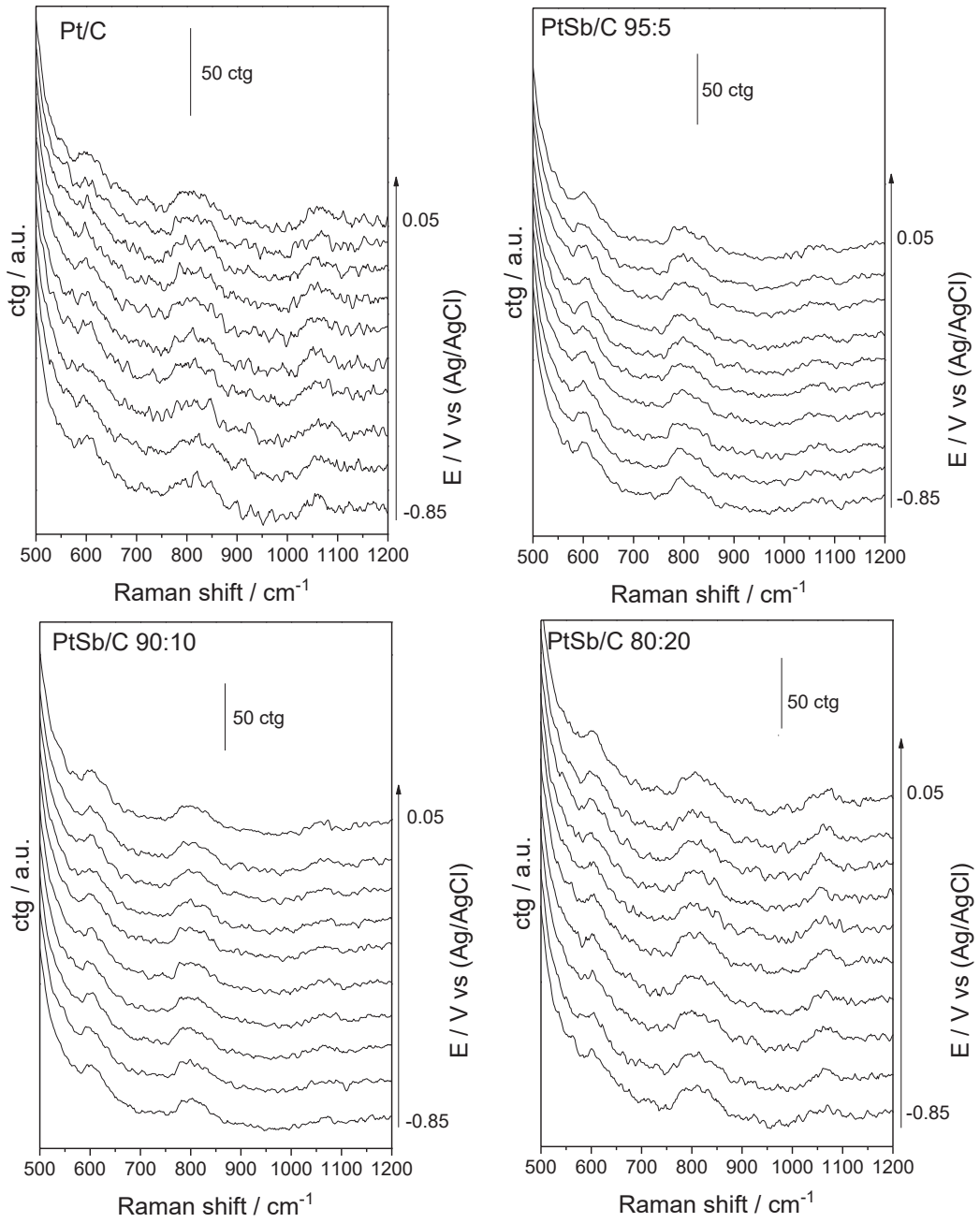

Fig. 11. In-Situ Raman spectra of electrochemical measurements of glycerol oxidation reaction in NaOH 1.0 mol L^{-1} + glycerol 1 mol L^{-1} on PtSb/C materials taken at −0.85 to 0.05 V.

Sb oxides, and to the synergic effect between alloyed platinum and antimony. PtSb/C catalysts favor the formation of 1,3-dihydroxy-2-propanone. In a next work, ternary PtSbM (M = N, Bi) electrocatalysts will be tested for the electrooxidation of glycerol.

Declaration of Competing Interest

The authors declare that they have no known competing financial interests or personal relationships that could have appeared to influence the work reported in this paper.

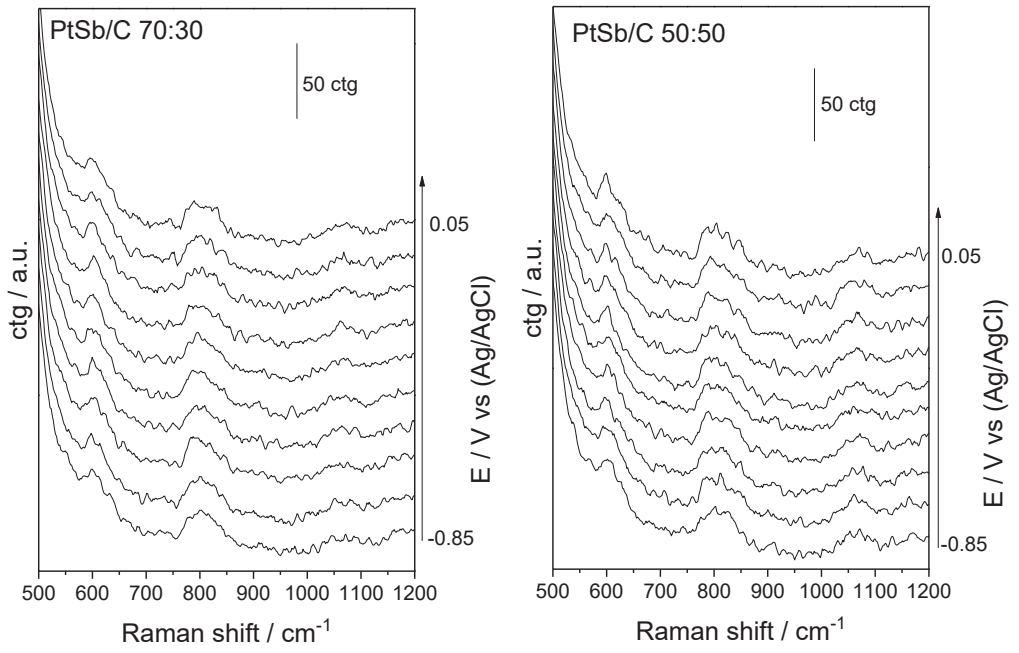

Fig. 11. (*continued*).

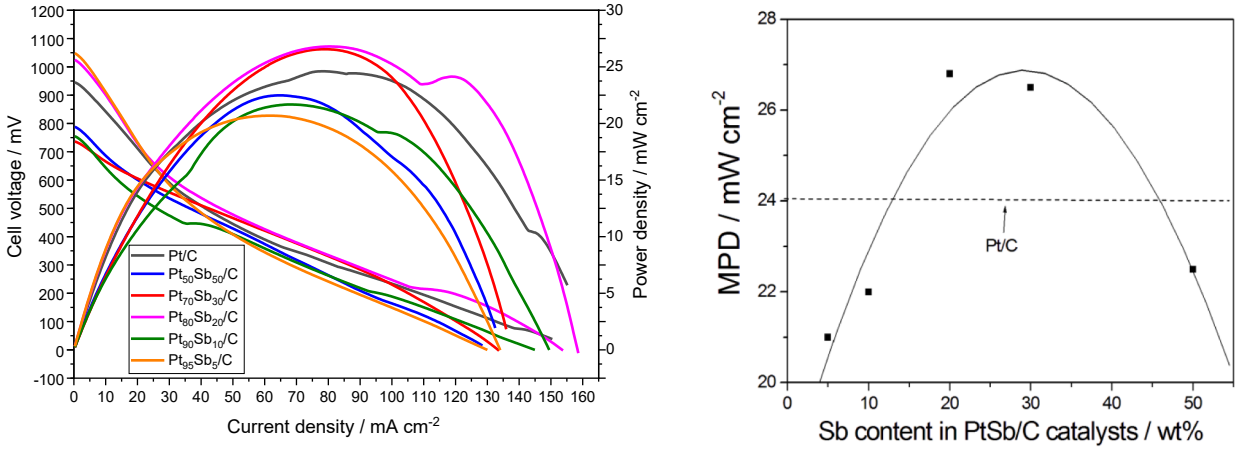

Fig. 12. (a) Direct glycerol fuel cell experiments for Pt/C, $Pt_{50}Sb_{50}$/C, $Pt_{70}Sb_{30}$/C, $Pt_{80}Sb_{20}$/C, $Pt_{90}Sb_{10}$/C and $Pt_{95}Sb_{5}$/C electrocatalysts. Flow = 1 mL min^{-1} of a 2 mol L^{-1} solution of NaOH in the presence of 2.0 mol L^{-1} of glycerol. The cathode was maintained under an oxygen flow of 150 mL min^{-1}. Cell operating temperature = 100 °C. Humidifier bottle temperature = 85 °C. (b) Dependence of the maximum power density (MPD) on Sb content in PtSb/C catalysts.

Acknowledgments

CAPES, CNPq (302709/2020-7), FAPESP (2017/11937-4) and CINE-SHELL (ANP) consented to the acknowledgement.

References

[1] R.L. Arechederra, B.L. Treu, S.D. Minteer, Development of glycerol/O2 biofuel cell, J. Power Sources 173 (1) (2007) 156–161.
[2] P. Sangkheaw, S. Therdthianwong, A. Therdthianwong, N. Wongyao, S. Yongprapat, Enhancement of anode performance for alkaline-acid direct glycerol fuel cells, Renewable Energy 161 (2020) 395–407.
[3] S. Lee, H.J. Kim, E.J. Lim, Y. Kim, Y. Noh, G.W. Huber, W.B. Kim, Highly selective transformation of glycerol to dihydroxyacetone without using oxidants by a PtSb/C-catalyzed electrooxidation process, Green Chem. 18 (9) (2016) 2877–2887.
[4] C. Coutanceau, S. Baranton, R.S.B. Kouame, Selective electrooxidation of glycerol into value-added chemicals: a short overview, Front Chem 7 (2019) 100.
[5] L. Yang, Y. Jiang, Z. Zhu, Z. Hou, Selective oxidation of glycerol over different shaped WO3 supported Pt NPs, Mol. Catal. 523 (2022), 111545.
[6] E.H. Fontes, C.E.D. Ramos, C.A. Ottoni, R.F.B. de Souza, E. Antolini, A.O. Neto, Glycerol dehydrogenation steps on Au/C surface in alkaline medium: An in-situ ATR-FTIR approach, Renewable Energy 167 (2021) 954–959.
[7] L. Yang, T. He, C. Lai, P. Chen, Z. Hou, Selective oxidation of glycerol with oxygen in base-free solution over N-doped-carbon-supported Sb@PtSb2 hybrid, Chin. J. Catal. 41 (3) (2020) 494–502.
[8] S.S. Siwal, S. Thakur, Q.B. Zhang, V.K. Thakur, Electrocatalysts for electrooxidation of direct alcohol fuel cell: chemistry and applications, Mater. Today Chem. 14 (2019), 100182.
[9] W. Wan, S.C. Ammal, Z. Lin, K.-E. You, A. Heyden, J.G. Chen, Controlling reaction pathways of selective C-O bond cleavage of glycerol, Nat. Commun. 9 (1) (2018) 4612.
[10] L. Zhang, D. Xia, Electrocatalytic activity of ordered intermetallic PtSb for methanol electro-oxidation, Appl. Surf. Sci. 252 (6) (2006) 2191–2195.
[11] X. Yu, P.G. Pickup, Pb and Sb modified Pt/C catalysts for direct formic acid fuel cells, Electrochim. Acta 55 (24) (2010) 7354–7361.

[12] R. Nie, D. Liang, L. Shen, J. Gao, P. Chen, Z. Hou, Selective oxidation of glycerol with oxygen in base-free solution over MWCNTs supported PtSb alloy nanoparticles, Appl. Catal. B 127 (2012) 212–220.
[13] C.A. Ottoni, S.G. da Silva, R.F.B. De Souza, A.O. Neto, Glycerol oxidation reaction using PdAu/C electrocatalysts, Ionics 22 (7) (2016) 1167–1175.
[14] J.C.M. Silva, L.S. Parreira, R.F.B. De Souza, M.L. Calegaro, E.V. Spinacé, A.O. Neto, M.C. Santos, PtSn/C alloyed and non-alloyed materials: Differences in the ethanol electro-oxidation reaction pathways, Appl. Catal. B 110 (2011) 141–147.
[15] R.F.B. De Souza, J.C.M. Silva, F.C. Simoes, M.L. Calegaro, A.O. Neto, M.C. Santos, New approaches for the ethanol oxidation reaction of Pt/C on carbon cloth using ATR-FTIR, Int J Electrochem Sci 7 (6) (2012) 5356–5366.
[16] R.S. Henrique, R.F.B. De Souza, J.C.M. Silva, J.M.S. Ayoub, R.M. Piasentin, M. Linardi, et al., Preparation of Pt/C-In 2O 3.SnO 2 electrocatalysts by borohydride reduction process for ethanol electro-oxidation, Int. J. Electrochem. Sci. 7 (3) (2012) 2036–2046.
[17] V.F. de Carmargo, E.H. Fontes, J. Nandenha, R.F.B. de Souza, A.O. Neto, High activity of Pt–Rh supported on C-ITO for ethanol oxidation in alkaline medium, Res. Chem. Intermed. 46 (2) (2020) 1555–1570.
[18] J.M.S. Ayoub, A.N. Geraldes, M.M. Tusi, E.V. Spinacé, A.O. Neto, Preparation of PtSnSb/C by an alcohol reduction process for direct ethanol fuel cell (DEFC), Ionics 17 (6) (2011) 559–564.
[19] D. Segets, L. Martinez Tomalino, J. Gradl, W. Peukert, Real-time monitoring of the nucleation and growth of ZnO nanoparticles using an optical hyper-rayleigh scattering method, J. Phys. Chem C 113 (28) (2009) 11995–12001.
[20] X. Yu, P.G. Pickup, Codeposited PtSb/C catalysts for direct formic acid fuel cells, J. Power Sources 196 (19) (2011) 7951–7956.
[21] B.V. Crist, Argon implanted into graphite, by XPS, Surf. Sci. Spectra 1 (4) (1992) 376–380.
[22] J. Cai, Y. Huang, Y. Guo, Facile synthesis of PdSbx/C nanocatalyst with high performance for ethanol electro-oxidation in alkaline medium, Int. J. Hydrogen Energy 39 (32) (2014) 18256–18263.
[23] R.G. Haverkamp, A.T. Marshall, B.C.C. Cowie, Energy resolved XPS depth profile of (IrO2, RuO2, Sb2O5, SnO2) electrocatalyst powder to reveal core-shell nanoparticle structure, Surf. Interface Anal. 43 (5) (2011) 847–855.
[24] M.C. Biesinger, B.P. Payne, A.P. Grosvenor, L.W.M. Lau, A.R. Gerson, R.S.C. Smart, Resolving surface chemical states in XPS analysis of first row transition metals, oxides and hydroxides: Cr, Mn, Fe, Co and Ni, Appl. Surf. Sci. 257 (7) (2011) 2717–2730.
[25] J.C. Castro, M.H.M.T. Assumpção, R.F.B. de Souza, E.V. Spinacé, A.O. Neto, Electro-Oxidation of Ethanol on PtSnRh/C-Sb2O5·SnO2 Electrocatalysts Prepared by Borohydride Reduction, Electrocatalysis 4 (3) (2013) 159–166.
[26] L. Guo, Z. Wu, T. Liu, W. Wang, H. Zhu, Synthesis of novel Sb2O3 and Sb2O5 nanorods, Chem. Phys. Lett. 318 (1) (2000) 49–52.
[27] J. Xu, D. Aili, Q. Li, C. Pan, E. Christensen, J.O. Jensen, W. Zhang, G. Liu, X. Wang, N.J. Bjerrum, Antimony doped tin oxide modified carbon nanotubes as catalyst supports for methanol oxidation and oxygen reduction reactions, J. Mater. Chem. A 1 (34) (2013) 9737.
[28] A. Falase, M. Main, K. Garcia, A. Serov, C. Lau, P. Atanassov, Electrooxidation of ethylene glycol and glycerol by platinum-based binary and ternary nano-structured catalysts, Electrochim. Acta 66 (2012) 295–301.
[29] D.Z. Jeffery, G.A. Camara, The formation of carbon dioxide during glycerol electrooxidation in alkaline media: First spectroscopic evidences, Electrochem. Commun. 12 (8) (2010) 1129–1132.
[30] Y. Kwon, S.C.S. Lai, P. Rodriguez, M.T.M. Koper, Electrocatalytic oxidation of alcohols on gold in alkaline media: base or gold catalysis? J. Am. Chem. Soc. 133 (18) (2011) 6914–6917.
[31] C.A. Ottoni, S.G. da Silva, R.F.B. De Souza, A.O. Neto, PtAu electrocatalyst for glycerol oxidation reaction using a ATR-FTIR/single direct alkaline glycerol/air cell in situ study, Electrocatalysis 7 (1) (2016) 22–32.
[32] M. Simões, S. Baranton, C. Coutanceau, Electro-oxidation of glycerol at Pd based nano-catalysts for an application in alkaline fuel cells for chemicals and energy cogeneration, Appl. Catal. B 93 (3–4) (2010) 354–362.
[33] J. Cai, H. Ma, J. Zhang, Z. Du, Y. Huang, J. Gao, J. Xu, Catalytic oxidation of glycerol to tartronic acid over Au/HY catalyst under mild conditions, Chin. J. Catal. 35 (10) (2014) 1653–1660.
[34] J. Schnaidt, M. Heinen, D. Denot, Z. Jusys, B.R. Jürgen, Electrooxidation of glycerol studied by combined in situ IR spectroscopy and online mass spectrometry under continuous flow conditions, J. Electroanal. Chem. 661 (1) (2011) 250–264.
[35] M. Simões, S. Baranton, C. Coutanceau, Enhancement of catalytic properties for glycerol electrooxidation on Pt and Pd nanoparticles induced by Bi surface modification, Appl. Catal. B 110 (2011) 40–49.
[36] C. Coutanceau, S. Baranton, R.S.B. Kouamé, Selective electrooxidation of glycerol into value-added chemicals: a short overview. Front. Chem. 7 (100) (2019).
[37] A.O. Neto, J. Nandenha, M.H.M.T. Assumpção, M. Linardi, E.V. Spinacé, R.F.B. de Souza, In situ spectroscopy studies of ethanol oxidation reaction using a single fuel cell/ATR-FTIR setup, Int. J. Hydrogen Energy 38 (25) (2013) 10585–10591.
[38] B. Liu, J. Greeley, Decomposition pathways of glycerol via C-H, O–H, and C–C bond scission on Pt(111): A density functional theory study, J. Phys. Chem. C 115 (40) (2011) 19702–19709.
[39] N. Worz, A. Brandner, P. Claus, Platinum−bismuth-catalyzed oxidation of glycerol: kinetics and the origin of selective deactivation, J. Phys. Chem. C 114 (2) (2010) 1164–1172.
[40] E. Antolini, Glycerol electro-oxidation in alkaline media and alkaline direct glycerol fuel cells, Catalysts 9 (12) (2019) 980.
[41] R.F.B. De Souza, É.T. Neto, M.L. Calegaro, E.A. Santos, H.S. Martinho, M.C. dos Santos, Ethanol electro-oxidation on Pt/C electrocatalysts: an “in situ” raman spectroelectrochemical study, Electrocatalysis 2 (1) (2011) 28–34.
[42] Y.-F. Huang, P.J. Kooyman, M.T.M. Koper, Intermediate stages of electrochemical oxidation of single-crystalline platinum revealed by in situ Raman spectroscopy, Nat. Commun. 7 (1) (2016) 12440.
[43] G.W. Graham, W.H. Weber, J.R. McBride, C.R. Peters, Raman investigation of simple and complex oxides of platinum, J. Raman Spectrosc. 22 (1) (1991) 1–9.
[44] G. Mestl, P. Ruiz, B. Delmon, H. Knozinger, Sb2O3/Sb2O4 in reducing/oxidizing environments: an in situ Raman spectroscopy study, J. Phys. Chem. C 98 (44) (1994) 11276–11282.